Radiology

# Multiparametric MR Imaging of Diffusion and Perfusion in Contrast-enhancing and Nonenhancing Components in Patients with Glioblastoma[1]

Natalie R. Boonzaier, PhD
Timothy J. Larkin, PhD
Tomasz Matys, MD, PhD
Anouk van der Hoorn, MD, PhD
Jiun-Lin Yan, MD
Stephen J. Price, BSc, MBBS(Hons), PhD,
    FRCS(Neuro Surg)

**Purpose:** To determine whether regions of low apparent diffusion coefficient (ADC) with high relative cerebral blood volume (rCBV) represented elevated choline (Cho)-to–*N*-acetylaspartate (NAA) ratio (hereafter, Cho/NAA ratio) and whether their volumes correlated with progression-free survival (PFS) and overall survival (OS) in patients with glioblastoma (GBM).

**Materials and Methods:** This retrospective analysis was approved by the local research ethics committee. Volumetric analysis of imaging data from 43 patients with histologically confirmed GBM was performed. Patients underwent preoperative 3-T magnetic resonance imaging with conventional, diffusion-weighted, perfusion-weighted, and spectroscopic sequences. Patients underwent subsequent surgery with adjuvant chemotherapy and radiation therapy. Overlapping low-ADC and high-rCBV regions of interest (ROIs) (hereafter, ADC-rCBV ROIs) were generated in contrast-enhancing and nonenhancing regions. Cho/NAA ratio in ADC-rCBV ROIs was compared with that in control regions by using analysis of variance. All resulting ROI volumes were correlated with patient survival by using multivariate Cox regression.

**Results:** ADC-rCBV ROIs within contrast-enhancing and nonenhancing regions showed elevated Cho/NAA ratios, which were significantly higher than those in other abnormal tumor regions ($P < .001$ and $P = .008$ for contrast-enhancing and nonenhancing regions, respectively) and in normal-appearing white matter ($P < .001$ for both contrast-enhancing and nonenhancing regions). After Cox regression analysis controlling for age, tumor size, resection extent, O-6-methylguanine-DNA methyltransferase-methylation, and isocitrate dehydrogenase mutation status, the proportional volume of ADC-rCBV ROIs in nonenhancing regions significantly contributed to multivariate models of OS (hazard ratio, 1.132; $P = .026$) and PFS (hazard ratio, 1.454; $P = .017$).

**Conclusion:** Volumetric analysis of ADC-rCBV ROIs in nonenhancing regions of GBM can be used to identify patients with poor survival trends after accounting for known confounders of GBM patient outcome.

Glioblastoma (GBM) is the most aggressive malignant primary brain tumor in adults, with its characteristic spatial and temporal intratumor heterogeneity (1) being at least partly responsible for dismal patient outcome. Current surgical treatment of GBM aims to remove the contrast material–enhanced component. Surrounding nonenhancing components, defined by T2-weighted signal hyperintensity, are largely left behind even though they harbor malignant tumor cells (2). This is done to avoid neurologic injury. Despite high-dose volume treatment, adjuvant radiation therapy applied to the nonenhancing component often fails to fully eliminate malignant cells, leading to local recurrence (3,4). Precise imaging details that underlie the nonenhancing component remain unclear and relatively unexplored.

Various imaging methods have been assessed to probe biologic properties underlying GBM; these include the use of relative cerebral blood volume (rCBV) (5–8), apparent diffusion coefficient (ADC) (7,9–14), or a combination thereof (7,15–17) to characterize tumor extent, guide resection, or yield prognostic information (18,19). ADC negatively correlates with cellularity in gliomas (10,13,20), and rCBV positively correlates with tumor vascularity (5) and cellular proliferation (21). With proton magnetic resonance (MR) spectroscopy ($^1$H), metabolic ratios of choline-containing compounds (Cho) to $N$-acetylaspartate (NAA) (hereafter, Cho/NAA ratio) correlate with tumor cellularity, proliferation (22,23), and infiltration (24), making the Cho/NAA ratio a reliable measure with which to analyze differences or similarities in tumor presence among regions of interest (ROIs).

Studies that focus on the nonenhancing component are limited (25–28). Volumetric properties of tissue with abnormal ADC and rCBV have not been extensively assessed in patients with GBM (29). In instances in which ADC and rCBV have been assessed (16), not all major confounding factors

of survival were included in multivariate regression models. In addition to age, these include extent of resection (30), enhancing tumor volume (31), O-6-methylguanine-DNA methyltransferase (MGMT)-methylation status (32), and isocitrate dehydrogenase-1 (IDH-1) mutation status (33).

Our hypothesis was that ROIs of low ADC (implying high cellularity) with intersecting high rCBV (implying vascularity) would metabolically represent regions of tumor presence, as determined with the Cho/NAA ratio. The overall purpose was to determine whether regions of low ADC with high rCBV indicated an elevated Cho/NAA ratio and whether their volumes correlated with progression-free survival (PFS) and overall survival (OS) in patients with GBM.

## Materials and Methods

### Patients

This study was approved by the local research ethics committee, and signed informed consent was obtained from each

---

### Advances in Knowledge

- Combining regions of low apparent diffusion coefficient (ADC) with intersecting regions of high relative cerebral blood volume (rCBV) in patients with glioblastoma (GBM) generates spatially distinct regions of interest (ROIs) that demonstrate a significantly elevated choline-to–$N$-acetylaspartate ratio in comparison with that in other regions of the tumor ($P$ = .008) and in contralateral normal-appearing white matter ($P$ < .001).

- The increased proportion of these ROIs within the nonenhancing component of GBM carries prognostic information and is associated with poor overall survival (OS) (log-rank $P$ = .017).

- After accounting for age, tumor volume, extent of resection, O-6-methylguanine-DNA methyltransferase-methylation status, and isocitrate dehydrogenase-1 mutation status, the proportion of these ROIs within nonenhancing regions significantly contributes to the model of OS (hazard ratio, 1.132; $P$ = .026) and progression-free survival (hazard ratio, 1.454; $P$ = .017).

---

### Implications for Patient Care

- Volumetric analysis of ADC and rCBV, especially within the nonenhancing component, could yield valuable patient-specific information about potential sites that are responsible for failure of chemotherapy and radiation therapy.

- Shifting focus from imaging features of the contrast-enhancing component to those of the nonenhancing component during individualized GBM assessment may result in the identification of regions that cannot be visualized with conventional MR imaging and that would be suited for targeted boost radiation therapy or extended surgical resection.

---

patient. Preoperative data from 47 patients (mean age, 58.6 years; age range, 28–75 years; 36 [76%] male patients) with subsequent histologic confirmation of GBM were prospectively collected (July 2010 to January 2012), and this was a retrospective analysis that included outcome data. Exclusion criteria were previous cranial surgery, cerebral radiation therapy, or another known primary brain tumor. A total of 53 patients underwent baseline imaging (Fig 1). Three (6%) patients withdrew from the study after baseline MR imaging, and three (6%) had grade III astrocytomas. Resection was performed, on average, within 1 day of imaging (range, 0–9 days). All patients were taking a stable dose (8 mg/d) of dexamethasone. Surgery was performed with 5-aminolevulinic acid fluorescence, with the aim of completely resecting the contrast-enhancing area. Thereafter, patients underwent radiation therapy with concomitant and adjuvant chemotherapy. The extent of resection was assessed as a binary outcome of complete or partial resection of the contrast-enhancing region on the basis of findings of an early (<72 hours) postoperative MR imaging study. Patients were observed, and the response assessment in neuro-oncology criteria was used to identify progression, with postsurgical imaging findings as the baseline (34). Outcome measures were determined retrospectively. The dates of progression and death were recorded to calculate PFS and OS (ie, the number of days after surgery), respectively. Thirty (64%) of 47 patients were previously included in a report on perfusion and diffusion tensor imaging of GBM (35). This article reports the results of volumetric analysis of intersecting threshold-defined ADC and rCBV while using the Cho/NAA ratio to compare imaging profiles of tumor presence.

## MR Image Acquisition

Imaging was performed with a 3-T Magnetom Trio unit (Siemens Healthcare, Erlangen, Germany). Imaging sequences included (a) a previously described (35) axial T2-weighted sequence (repetition time msec/echo time msec, 4840–5470/114; refocusing pulse flip angle, 150°; field of view, 220 × 165 mm; 23–26

### Figure 1



**Figure 1:** Flowchart shows how patients were excluded. Six patients were excluded because of criteria set a priori. The remaining patients were excluded because of criteria set retrospectively. These included an ADC-rCBV ROI with a volume smaller than 50% of the chemical shift imaging voxel (2 $cm^3$), an ADC-rCBV ROI located outside the chemical shift imaging grid, and a Cramer-Rao lower bound greater than 20%. All qualifying chemical shift imaging voxel values were recorded for ADC-rCBV ROIs; this resulted in 41 voxels from 20 patients in contrast-enhancing regions and 43 voxels from 23 patients in nonenhancing regions.

sections; 0.5-mm section gap; voxel size, 0.7 × 0.7 × 5.0 mm; acquisition time, 93 seconds), (b) a T2-weighted fluid-attenuated inversion recovery sequence (repetition time msec/echo time msec/inversion time msec, 7840–8420/95/2500; refocusing pulse flip angle, 150°; field of view, 250 × 200 mm; 27 sections; 1-mm section gap; voxel size, 0.8 × 0.8 × 4.0 mm; acquisition time, 268 seconds), (c) diffusion-tensor imaging with a single-shot echo-planar sequence (8300/98; flip angle, 90°; field of view, 192 × 192 mm; 63 sections; no section gap; voxel size, 2.0 × 2.0 × 2.0 mm; acquisition time, 566 seconds) and with inline ADC calculation using b values of 0–1000 sec/$mm^2$ to generate ADC parameters that reflect general clinical practice, (d) a postcontrast dynamic susceptibility contrast enhancement sequence (1500/30;

flip angle, 90°; field of view, 192 × 192 mm; 19 sections; section gap, 1.5 mm; voxel size, 2.0 × 2.0 × 5.0 mm; acquisition time, 141 seconds) with 9 mL of gadobutrol (1.0 mmol/mL, Gadovist; Bayer Schering Pharma, Berlin, Germany) followed by a 20-mL saline flush administered via a power injector at a rate of 5 mL/sec, (e) a three-dimensional T1-weighted sequence with gadoluium chelate injection (Gadovist; Bayer Schering Pharma) (900/2.98/900; flip angle, 9°; field of view, 256 × 240 mm; 176–208 sections; no section gap; voxel size, 1.0 × 1.0 × 1.0 mm; acquisition times, 252 and 554 seconds), and (f) multivoxel two-dimensional $^1$H MR spectroscopy chemical-shift imaging with a semilocalized by adiabatic selective refocusing pulse sequence (2000/30–35; flip angle, 90°; field of view, 160 × 160 mm; voxel size,
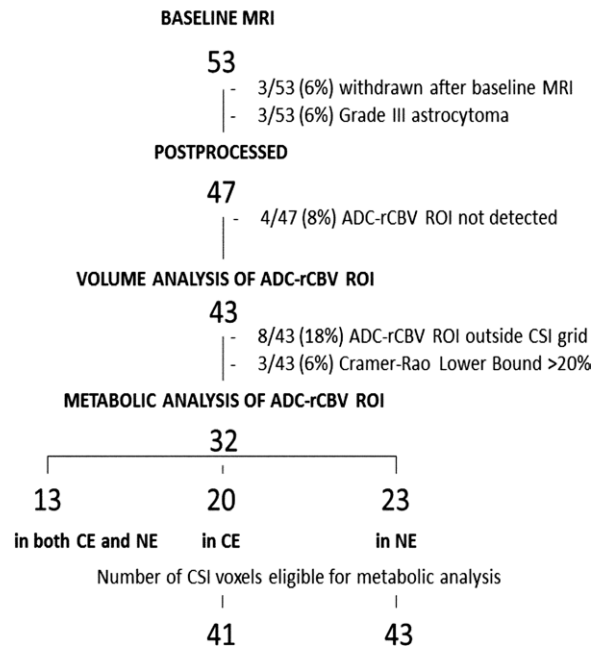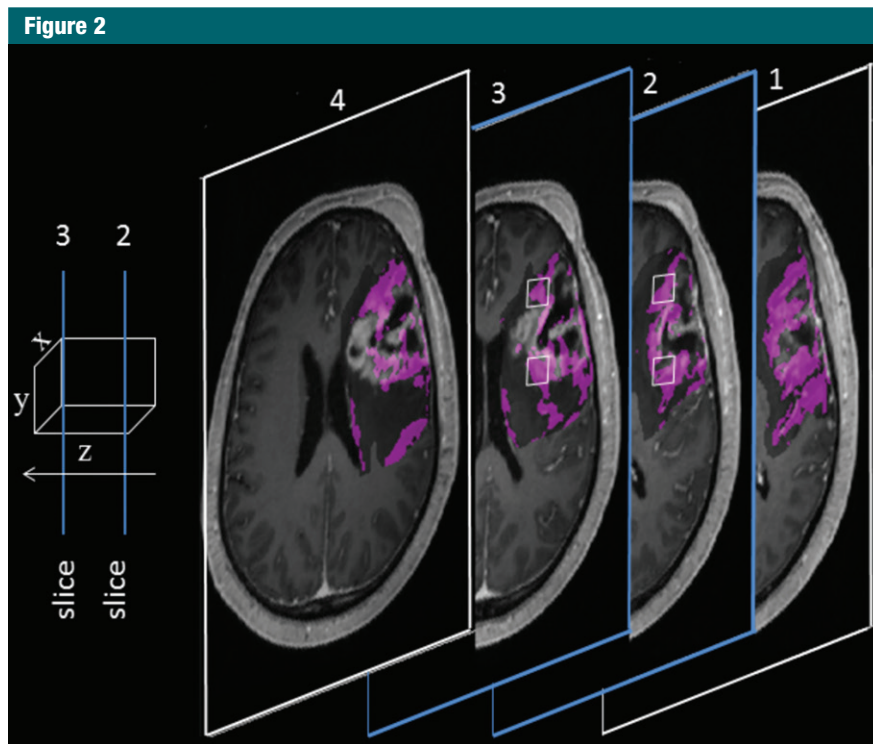
## Figure 2



**Figure 2:** T1-weighted contrast-enhanced MR image set shows how chemical shift imaging voxels were included for analysis and where the ROI (magenta) was present inside the voxels along the x-, y-, and z-axes.

10 × 10 × 15–20 mm; acquisition time, 486 seconds).

### Image Processing and ROI Selection

All images were coregistered to the T2-weighted images by using an affine transformation with the Functional MRI of the Brain (or FMRIB) Linear Image Registration Tool (or FLIRT) in FMRIB Software Library (FMRIB, Oxford, England). T2-weighted images were used to guide spectroscopic data acquisition. Spectroscopy data were processed with the LCModel (Provencher, Oakville, Ontario, Canada). All relevant spectra from chemical shift imaging voxels of interest were assessed for artifacts by using previously published criteria (36). The values of the Cramer-Rao lower bounds were used to evaluate the quality and reliability of chemical shift imaging data, and values with a standard deviation greater than 20% were discarded. Dynamic susceptibility contrast-enhanced data were processed offline by using NordicICE (NordicNeuroLab, Bergen, Norway). Maps

of rCBV were generated after contrast agent leakage correction, and they were based on the Boxerman (37) description. A standard population-based arterial input function was automatically defined in the NordicICE (NordicNeuroLab) software, and it was applied in a global manner. As ADC values are dependent on the $b$ value, ADC images were normalized to the contralateral normal-appearing white matter mean.

ADC and rCBV voxel data were pooled, and thresholds were established by using the histogram percentile values with Matlab software (MathWorks, Natick, Mass). Previously, high rCBV percentile values have ranged from 75% to 90% for image-guided biopsy studies of glioma heterogeneity (21). Thus, the rCBV threshold was taken in a stepwise manner from the 85th percentile within the contrast-enhancing component. After initial inspection, it was decided that if the resulting ADC-rCBV ROIs were too small for spectroscopic analysis, less than half the volume (1 cm³) of the spectroscopy

voxel, the 75th or 65th percentile of pooled rCBV voxels, would be used. Previously, ADC percentile values have ranged from 10% to 25% for analysis of heterogeneity (38) or texture (39) and survival (14). Thus, prior to inspection of data, the low ADC threshold was taken at the 15th percentile of the pooled voxels. Overlapping low ADC and high rCBV voxels were defined as ADC-rCBV ROIs. Because this method of threshold selection is specific, it must be determined whether overall conclusions of this study exclusively depended on the method of threshold establishment. To address this, test ROIs were generated by using percentile values for each individual patient. Thus, two sets of ADC-rCBV ROIs were compared with those in control subjects. These were main ROIs, which were generated with thresholds that were extracted on a pooled-value basis by using data from all patients, as described previously, and test ROIs, which were generated with thresholds that were extracted on an individual basis, per patient. Test ROI volumes were generated to be compared with main ROI volumes and to undergo the same statistical analyses of survival. When referring to ADC-rCBV ROIs throughout this article, we refer to the main ROIs.

The contrast-enhancing regions were segmented by using semiautomated software (GeoS; Microsoft Research, Cambridge, England). Unenhanced regions were manually segmented with ImageJ software (National Institutes of Health, Bethesda, Md). A neuroradiologist with more than 4 years of experience (T.M.) segmented the test regions for interrater reliability testing. The Dice similarity coefficient score was applied to presence and absence data and was used to compare the new test ROI mask data against the original reference mask, which was segmented by the initial reader (N.R.B., >3 years of brain tumor image analysis experience). The superimposed ^{1}H MR spectroscopy data were analyzed as described previously (35). Only chemical shift imaging voxels in which the ROIs continued down the z-axis were included (Fig 2). The z-axis data were incorporated to further ensure that metabolite values recorded for the ADC-rCBV ROIs were due
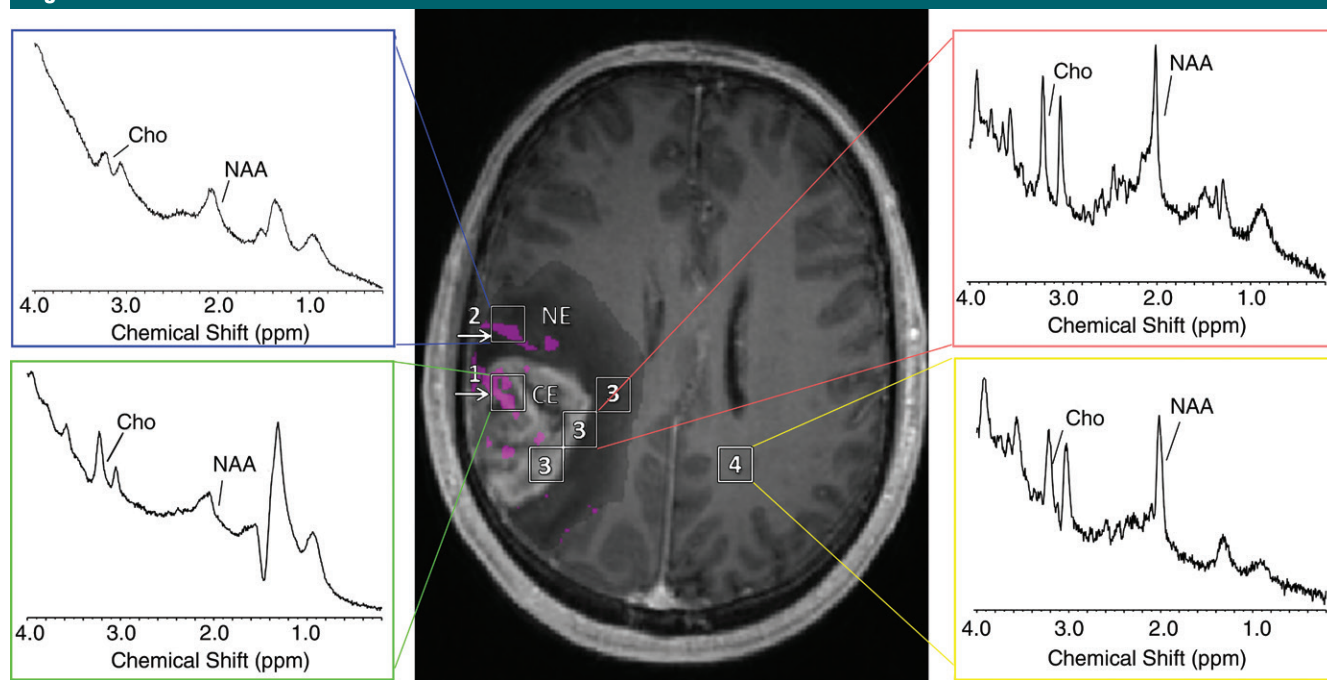
Radiology

**Figure 3**

**Figure 3:** T1-weighted contrast-enhanced MR image shows the four regions for metabolic assessment, with example spectra of NAA at 2.0 and Cho at 3.2. Examples include the ADC-rCBV ROI (magenta) in a chemical shift imaging voxel with a Cho/NAA ratio of 1.8 in the contrast-enhanced area *(1)* and 0.6 in the unenhanced area *(2)*. Also shown are example spectra of an abnormal control region that does not meet the ROI criteria of low ADC with intersecting high rCBV *(3)* with a Cho/NAA ratio of 0.3 and normal-appearing white matter *(4)* with a Cho/NAA ratio of 0.2.

to the presence of that ROI and were not due to the surrounding non-ROI regions colocalizing the chemical shift imaging voxel. As the ADC-rCBV ROIs were characterized by using Cho/NAA ratios, the control regions were based on chemical shift imaging voxels. Two sets of controls were identified by using chemical shift imaging voxels. These were *(a)* abnormal control regions, which were voxels within contrast-enhancing and nonenhancing areas that did not meet the ADC-rCBV ROI criteria, and *(b)* contralateral normal-appearing white matter. Regions for analysis included these two control regions: ADC-rCBV ROIs in contrast-enhancing regions and ADC-rCBV ROIs in nonenhancing regions (Fig 3). Lastly, the ADC-rCBV ROI volume and the conventional ROI volume were calculated by using Matlab software (Mathworks).

### Statistical Analysis

Data were analyzed with IBM SPSS software (version 22.0; IBM, Armonk, NY)

at a two-sided significance level of $\alpha$ = .05. Cho/NAA ratios were not normally distributed, and a log transformation was applied prior to analysis of variance, with posthoc analysis with Bonferroni correction used for multiple comparisons. Cho/NAA data were not normally distributed, and log transformation was applied prior to analysis of variance. After Bonferroni correction for multiple comparisons, the adjusted significance level among the location groups was $\alpha$ = .008 (.05/6 = .008). All volume data were not normally distributed and were log transformed prior to statistical testing. Differences in volume between the main ROIs and the test ROIs were explored by using the Student $t$ test, as all test ROIs were significantly larger than their respective main ROIs. Correlations between ROI volume and their corresponding conventional region volume were explored by using Pearson correlation. Volumes were dichotomized as high or low by using the median. Kaplan-Meier statistics analyzed survival as

a function of ROI volume and proportional ROI volume (percentage of conventional lesion, contrast-enhancing or nonenhancing). Cox regression accounted for confounders of GBM survival: age, contrast-enhancing volume, IDH-1 mutation status, MGMT-methylation status, and extent of resection. To compare relative accuracies for association with median OS and PFS, receiver operating characteristic curves were generated for ROI volumes. Their accuracies were compared with the area under the receiver operating characteristic curve.

### Results

Interrater variability of the manually segmented regions showed good agreement, with a mean Dice similarity coefficient score of 0.88 ± 0.04 (standard deviation). Complete resection of the contrast-enhancing region was achieved in 38 (81%) of 47 patients, while the remaining nine patients underwent partial resection. Median OS was

### Table 1

**Cho/NAA Ratios within the Four Locations**

| | | Descriptive | | Difference | | | | | |
| | | | | ROI in NE | | Control | | NAWM | |
| Region | No. of Voxels Tested | Mean ± Standard Deviation | 95% CI | Estimated Difference | P Value | Estimated Difference | P Value | Estimated Difference | P Value |
|---|---|---|---|---|---|---|---|---|---|
| ROI in CE | 41 | 0.291 ± 0.153 | 0.243, 0.334 | 0.072 (0.024) | .017 | 0.151 (0.025) | <.001* | 0.187 (0.024) | <.001* |
| ROI in NE | 43 | 0.220 ± 0.137 | 0.178, 0.262 | … | … | 0.079 (0.024) | .008* | 0.115 (0.024) | <.001* |
| Control | 38 | 0.140 ± 0.048 | 0.124, 0.156 | … | … | … | … | 0.036 (0.025) | .921 |
| NAWM | 39 | 0.104 ± 0.039 | 0.092, 0.118 | … | … | … | … | … | … |

Note.—Data in parentheses are the standard error. CE = contrast-enhancing area, NAWM = normal-appearing white matter, NE = nonenhancing area.

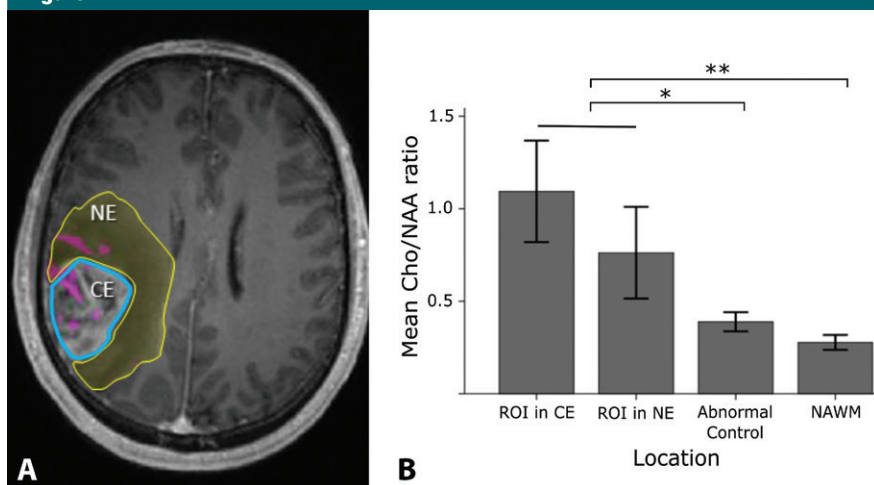* Adjusted significance level $\alpha$ .05/6 = .0083.

### Figure 4



**Figure 4:** *A,* MR image shows boundaries of contrast enhancement *(CE)* (blue) and nonenhancement *(NE)* (yellow) used to categorize the ADC-rCBV ROI (magenta) Cho/NAA ratio according to location. *B,* Means plot shows results from the posthoc homogeneous subset tests, with Cho/NAA ratio from contrast-enhanced and unenhanced areas in a separate subset from Cho/NAA ratio from abnormal control tumor regions and normal-appearing white matter *(NAWM)*. Lines extending from the bars show standard error of the mean. * = *P* < .01, ** = *P* < .001.

326 days (range, 27–1193 days). Median PFS was 224 days (range, 27–1130 days).

#### Regions of Interest

The thresholds of the 85th percentile rCBV (rCBV = 4.4) and the 75th percentile rCBV (rCBV = 3.4) generated ADC-rCBV ROIs that were too small for metabolic analysis. Thus, the 65th percentile rCBV (rCBV = 2.7) and the 15th percentile ADC (normalized threshold, 1.2) were used to generate ROIs. The ADC-rCBV ROIs were present in 43 (92%) of 47 patients and were situated outside the chemical shift imaging grid in eight (18%) of 43 patients. NAA values were unusable in three (6%) of 43 patients because the Cramer-Rao lower bounds standard deviation was greater than 20%. Thus, the sample size for metabolic assessment was 32 patients. Chemical shift imaging voxels colocalized with ADC-rCBV ROIs in contrast-enhancing regions in 20 (62%) of 32 patients, with a total of 41 voxels analyzed. Chemical shift imaging voxels colocalized with ADC-rCBV ROIs in nonenhancing regions in 23 (71%) of 32 patients, with a total of 43 voxels analyzed. Chemical shift imaging voxels colocalized with ADC-rCBV ROIs in both contrast-enhancing and nonenhancing regions in 13 (40%) of 32 patients. In the 32 patients, a total of 38 eligible chemical shift imaging voxels were identified within the abnormal control regions, and 39 eligible chemical shift imaging voxels were identified in the contralateral normal-appearing white matter.

#### Regions for Analysis

The Cho/NAA ratios of ADC-rCBV ROIs located in contrast-enhancing and nonenhancing regions were similar (95% confidence interval [CI]: 0.008, 0.136; *P* = .017) (Table 1, Fig 4). Both were significantly greater than that in the abnormal control region (95% CI: 0.086, 0.217; *P* < .001 for contrast-enhancing region) (95% CI: 0.015, 0.144; *P* = .008 for nonenhancing region). The Cho/NAA ratio of ADC-rCBV ROIs in contrast-enhancing and nonenhancing regions was significantly greater than that in normal-appearing white matter (95% CI: 0.122, 0.252; *P* < .001 for contrast-enhancing region) (95% CI: 0.051, 0.179; *P* < .001 for nonenhancing region). No significant difference in Cho/NAA ratio was detected between the abnormal control region and normal-appearing white matter (95% CI: −0.031, 0.102; *P* = .921).

## Table 2

### ROI Volumes and Relevant Patient Characteristics

| Parameter | No. of Patients | Total ROI Mean ± SD | P Value | ROI in CE Mean ± SD | P Value | ROI in NE Mean ± SD | P Value |
|---|---|---|---|---|---|---|---|
| | | Volume (cm³) | | | | | |
| Total volume | ... | 46.50 ± 67.70 | ... | 18.56 ± 33.50 | ... | 26.86 ± 36.11 | ... |
| Age at diagnosis | | | | | | | |
|   <60 y | 14 | 21.10 ± 27.08 | .053 | 12.13 ± 21.62 | .213 | 8.44 ± 9.13 | .016 |
|   ≥60 y | 29 | 58.12 ± 95.19 | … | 20.88 ± 45.54 | … | 35.60 ± 49.06 | … |
| Sex | | | | | | | |
|   Male | 32 | 50.38 ± 9260 | .740 | 19.90 ± 44.73 | .635 | 29.09 ± 47.71 | .896 |
|   Female | 11 | 33.51 ± 28.36 | … | 12.60 ± 15.52 | … | 19.94 ± 20.50 | … |
| Extent of resection | | | | | | | |
|   Complete | 34 | 35.38 ± 53.80 | .107 | 14.35 ± 27.12 | .258 | 20.07 ± 28.95 | .062 |
|   Partial | 9 | 86.42 ± 142.4 | … | 31.96 ± 69.26 | … | 52.00 ± 71.18 | … |
| MGMT-methylation status* | | | | | | | |
|   Methylated | 16 | 61.99 ± 110.3 | .952 | 25.36 ± 53.44 | .404 | 34.81 ± 57.05 | .895 |
|   Unmethylated | 24 | 38.06 ± 60.22 | … | 13.21 ± 28.64 | … | 23.81 ± 32.31 | … |
| IDH-1 mutation status† | | | | | | | |
|   Mutant | 1 | 79.67 | … | 68.16 | … | 0.11 | … |
|   Wild type | 42 | 45.26 ± 81.91 | … | 16.84 ± 38.98 | … | 27.12 ± 42.83 | … |
| | | Volume Proportion (%) | | | | | |
| Age at diagnosis | | | | | | | |
|   <60 y | 14 | 3.86 ± 7.53 | .443 | 6.31 ± 11.81 | .875 | 1.97 ± 2.86 | .027 |
|   ≥60 y | 29 | 5.12 ± 6.95 | … | 5.73 ± 7.80 | … | 5.64 ± 7.48 | … |
| Sex | | | | | | | |
|   Male | 32 | 5.16 ± 7.91 | .570 | 5.79 ± 9.77 | .595 | 4.90 ± 7.34 | .465 |
|   Female | 11 | 3.42 ± 3.75 | … | 6.28 ± 7.48 | … | 3.11 ± 3.22 | … |
| Extent of resection | | | | | | | |
|   Complete | 34 | 4.48 ± 6.94 | .710 | 5.82 ± 9.46 | .797 | 3.92 ± 5.76 | .478 |
|   Partial | 9 | 5.58 ± 7.98 | … | 6.27 ± 8.38 | … | 6.43 ± 9.08 | … |
| MGMT methylation status* | | | | | | | |
|   Methylated | 16 | 5.94 ± 8.38 | .418 | 7.32 ± 10.70 | .353 | 5.59 ± 7.29 | .434 |
|   Unmethylated | 24 | 3.92 ± 6.27 | … | 4.61 ± 7.43 | … | 3.96 ± 6.39 | … |
| IDH-1 mutation status† | | | | | | | |
|   Mutant | 1 | 27.12 | … | 39.52 | … | 9.77 | … |
|   Wild type | 42 | 4.18 ± 6.23 | … | 5.12 ± 7.59 | … | 4.32 ± 6.57 | … |

Note.—CE = contrast-enhancing area, NE = nonenhancing area, SD = standard deviation.

* MGMT-methylation status was unavailable in three patients.

† Only one patient with IDH-1 mutation; mean ± SD of original data.

As ADC-rCBV ROIs were absent or smaller than 1 cm³ in four (8%) of 47 patients, volumetric analysis was performed in 43 patients for raw and proportional volumes (Table 2). Both ADC-rCBV ROI volume (estimated difference, 0.636; standard error, 0.242; 95% CI: −1.139, 1.133; P = .016) and proportion of ADC-rCBV ROI (estimated difference, 0.039; standard error, 0.049; 95% CI: −0.159, 0.010; P = .027, respectively) in nonenhancing regions were significantly larger in patients older than 60 years. In 30 (70%) of 43 patients, ADC-rCBV ROIs were larger in nonenhancing regions than in contrast-enhancing regions (estimated difference, 0.510; standard error, 0.095; 95% CI: −0.704, 0.322; P < .001). The ADC-rCBV ROI volume inside the contrast-enhancing region positively correlated with contrast-enhancing volume (r = 0.291, P = .014). ADC-rCBV ROI volume inside the nonenhancing region positively correlated with nonenhancing volume (r = 0.350, P = .021). Total ADC-rCBV ROI volume and total lesion volume did not correlate (r = 0.291, P = .059). The differences between main ROIs and test ROIs are described in Table 3.

## Table 3

### Volume Differences between Main ROIs and Test ROIs

| ROI | Original and Log-transformed Data* | | Difference (Log-transformed data) | | | |
| --- | --- | --- | --- | --- | --- | --- |
| | Normalized Global Threshold (Main ROI) | Individualized Percentile Threshold (Test ROI) | Estimated Difference | 95% CI | t Statistic | P Value |
| Total ROI volume | | | | | | |
| Original volume/value | 46.503 ± 67.709 | 78.367 ± 50.594 | … | … | … | … |
| Log-transformed value | 3.140 ± 0.850 | 3.777 ± 0.361 | −0.641 (0.128) | −0.899, −0.382 | −4.998 | <.001 |
| ROI volume in CE | | | | | | |
| Original volume/value | 18.563 ± 33.504 | 19.546 ± 18.623 | … | … | … | … |
| Log-transformed value | 2.440 ± 1.054 | 3.061 ± 0.504 | −0.626 (0.146) | −0.921, −0.331 | −4.227 | <.001 |
| ROI volume in NE | | | | | | |
| Original volume/value | 26.864 ± 36.114 | 57.142 ± 44.648 | … | … | … | … |
| Log-transformed value | 2.948 ± 0.801 | 3.556 ± 0.530 | −0.608 (0.125) | −0.861, −0.355 | −4.855 | <.001 |
| Proportion total ROI CE + NE | | | | | | |
| Original/proportion value | 5.105 ± 7.055 | 6.392 ± 1.953 | … | … | … | … |
| Log-transformed value | 0.521 ± 0.431 | 0.854 ± 0.115 | −0.333 (0.070) | −0.474, −0.193 | −4.788 | <.001 |
| Proportion ROI CE | | | | | | |
| Original/proportion value | 6.574 ± 8.860 | 7.618 ± 5.879 | … | … | … | … |
| Log-transformed value | 0.553 ± 0.482 | 0.839 ± 0.305 | −0.286 (0.076) | −0.439, −0.133 | −3.774 | <.001 |
| Proportion ROI NE | | | | | | |
| Original/proportion value | 5.030 ± 7.213 | 7.550 ± 5.711 | … | … | … | … |
| Log-transformed value | 0.519 ± 0.414 | 0.862 ± 0.247 | −0.343 (0.075) | −0.494, −0.191 | −4.568 | <.001 |

Note.—Data in parentheses are the standard error. Main ROI is the normalized threshold using an ADC cutoff of 1.2 and an rCBV cutoff of 2.7. The test ROI is the individualized thresholds based on the 15th percentile ADC and the 65th percentile rCBV, per patient. CE = contrast-enhancing area, NE = nonenhancing area.

* Data are mean ± standard deviation.

### Survival Statistics

After univariate analysis, the volume of ADC-rCBV ROI in contrast-enhancing regions was associated with poor OS (log-rank $P$ = .040) (Table 4). The proportion of contrast-enhancing and nonenhancing regions with ADC-rCBV ROI was associated with poor OS (log-rank $P$ = .010), and the proportion of nonenhancing regions with ADC-rCBV ROI was associated with poor OS (log-rank $P$ = .017) (Fig 5). Assessment of age, contrast-enhancing volume, IDH-1 mutation, MGMT-methylation status, and extent of resection independently showed that only extent of resection had a significant association with both OS ($P$ = .022) and PFS ($P$ = .041). After we accounted for all the previously mentioned confounders and censored four cases with no recorded date of progression or death, the proportion of nonenhancing regions with ADC-rCBV ROI (hazard ratio, 1.132; $P$ = .026), extent of resection (hazard ratio, 0.090; $P$ = .011), and IDH-1 mutation status (hazard ratio, 0.010; $P$ = .008)

significantly contributed to the multivariate model of OS. The proportion of nonenhancing regions with ADC-rCBV ROI (hazard ratio, 1.454; $P$ = .017), extent of resection (hazard ratio, 0.013; $P$ = .031), and IDH-1 mutation status (hazard ratio, 0.000; $P$ = .011) significantly contributed to the multivariate model of PFS.

Cox regression results for test ROIs and main ROIs were similar. The proportion of nonenhancing regions with ADC-rCBV ROI (hazard ratio, 1.179; $P$ = .014), extent of resection (hazard ratio, 0.113; $P$ = .018), and IDH-1 mutation status (hazard ratio, 0.001; $P$ = .003) significantly contributed to the multivariate model of OS. In the analysis of PFS, the proportion of nonenhancing regions with ADC-rCBV ROI (hazard ratio, 1.149; $P$ = .050), extent of resection (hazard ratio, 0.073; $P$ = .011), and IDH-1 mutation status (hazard ratio, 0.004; $P$ = .007) were significant contributors. The proportion of ADC-rCBV ROI in nonenhancing regions was the only variable with significant association with median OS (area under the

receiver operating characteristic curve, 0.717; $P$ = .034) (Fig 6).

### Discussion

This study has shown that low-ADC ROIs with intersecting high rCBV depict ^{1}H MR spectroscopy features that suggest tumor presence in both contrast-enhancing and nonenhancing regions, and an increased proportion of these ROIs within the nonenhancing region is associated with poor patient survival. The nonenhancing component is typically left behind after surgical resection of the contrast-enhancing component; therefore, studies of this nature can offer insight into the subregions that may be responsible for local GBM recurrence.

Although previous studies have suggested use of an rCBV greater than 3 to identify tumor in the contrast-enhancing area (9,16), a reduced threshold was considered reasonable for assessment outside the contrast-enhancing area, where median rCBV values typically

**Table 4**

**Survival Statistics**

| Variable and Test | PFS | | | | OS | | | |
|---|---|---|---|---|---|---|---|---|
| | Hazard Ratio | 95% CI | AUC | *P* Value | Hazard Ratio | 95% CI | AUC | *P* Value |
| Total ROI volume | | | | | | | | |
| Log-rank test | … | … | … | .076 | … | … | … | .270 |
| Cox regression | 1.000 | 1.000, 1.000 | … | .254 | 1.000 | 1.000, 1.000 | … | .224 |
| ROC | … | 0.384, 0.816 | 0.600 | .351 | … | 0.433, 0.824 | 0.629 | .207 |
| ROI volume in CE | | | | | | | | |
| Log-rank test | … | … | … | .076 | … | … | … | .040* |
| Cox regression | 1.000 | 1.000, 1.000 | … | .483 | 1.000 | 1.000, 1.000 | … | .327 |
| ROC | … | 0.356, 0.786 | 0.571 | .507 | … | 0.398, 0.793 | 0.596 | .349 |
| ROI volume in NE | | | | | | | | |
| Log-rank test | … | … | … | .230 | … | … | … | .509 |
| Cox regression | 1.000 | 1.000, 1.000 | … | .125 | 1.000 | 1.000, 1.000 | … | .165 |
| ROC | … | 0.351, 0.787 | 0.569 | .520 | … | 0.437, 0.827 | 0.632 | .195 |
| Proportion total ROI (in CE and NE) | | | | | | | | |
| Log-rank test | … | … | … | .076 | … | … | … | .010* |
| Cox regression | 1.037 | 0.971, 1.108 | … | .281 | 1.064 | 0.976, 1.159 | … | .160 |
| ROC | … | 0.419, 0.843 | 0.631 | .221 | … | 0.437, 0.827 | 0.632 | .195 |
| Proportion ROI in CE | | | | | | | | |
| Log-rank test | … | … | … | .614 | … | … | … | .637 |
| Cox regression | 1.046 | 0.977, 1.120 | … | .196 | 1.039 | 0.974, 1.109 | … | .248 |
| ROC | … | 0.382, 0.809 | 0.596 | .373 | … | 0.347, 0.749 | 0.548 | .640 |
| Proportion ROI in NE | | | | | | | | |
| Log-rank test | … | … | … | .067 | … | … | … | .017* |
| Cox regression | 1.454 | 1.000, 1.000 | … | .017 | 1.132 | 1.015, 1.263 | … | .026* |
| ROC | … | 0.485, 0.901 | 0.693 | .071 | … | 0.541, 0.893 | 0.717 | .034* |

Note.—Cox-regression model accounting for patient age, enhancing tumor volume, MGMT-methylation status, IDH-1 mutation status, and extent of resection. AUC = area under the receiver operating characteristic curve, CE = contrast-enhancing area, NE = nonenhancing, and ROC = receiver operating characteristic curve.

* *P* value indicates a significant difference.

are lower (9,40). Additionally, a previous study (40) has suggested use of a threshold identical to that reported here for biopsy sampling within the contrast-enhancing area in the region with the highest rCBV, from 2.7 (9). A low-ADC threshold was used because of its inverse association with tumor cellularity, proliferation, and architectural disruption in nonenhancing areas (9,10,13). As the ADC threshold was generated from voxels in contrast-enhancing areas and from those in nonenhancing areas, its normalized value was not expected to be less than 1.00. However, this finding is in accordance with findings of a previous study that inversely correlated ADC with cellularity with a pooled mean ADC minimum of 1.2 ($r = 0.77$, $P = .007$) (13). Previous work using Cho and NAA has yielded findings in accordance with those
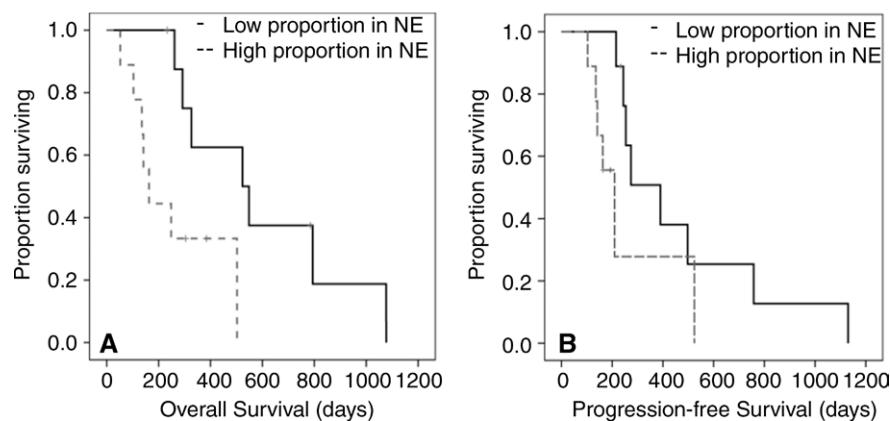
**Figure 5**



**Figure 5:** Kaplan-Meier plots show larger proportions of ADC-rCBV ROI in nonenhancing *(NE)* areas, *A,* were associated with worse OS (*P* = .017) and, *B,* trended with poor PFS (*P* = .067). Volumes were categorized as high or low by using relevant median values.
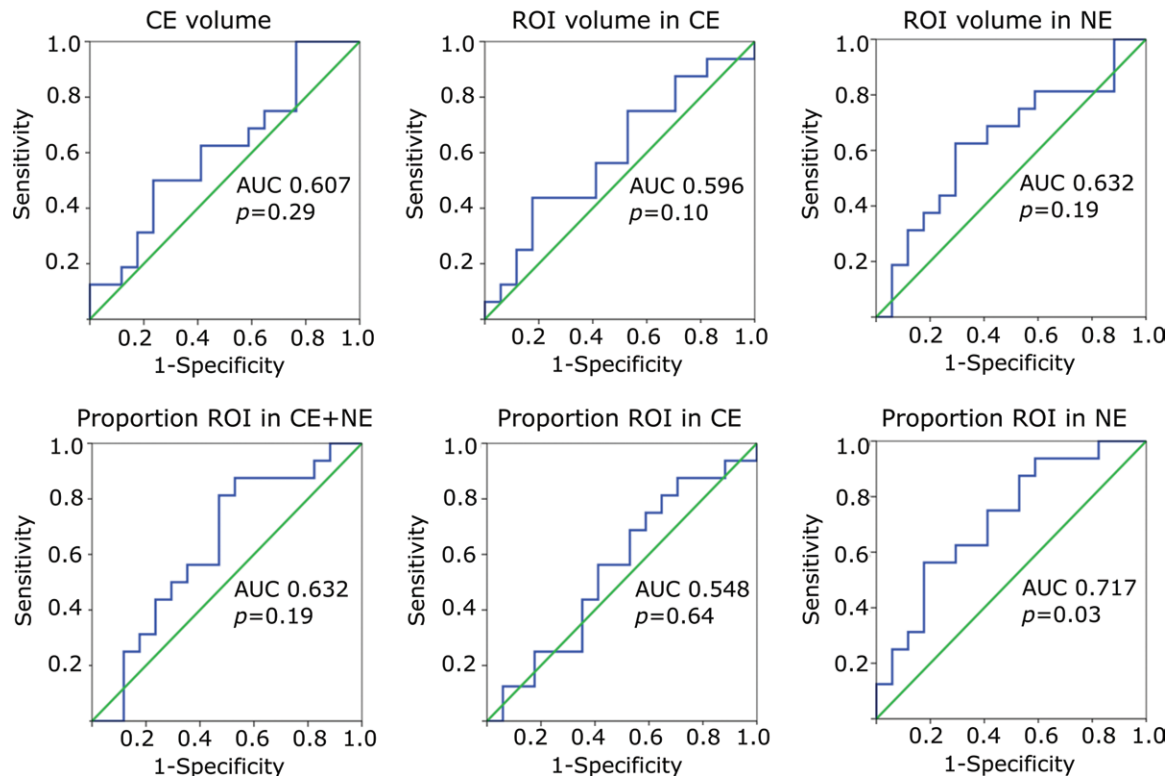
**Figure 6:** Receiver operating characteristic curves compare relative accuracies in association between ADC-rCBV ROI volumes and proportions with median OS. The only measure with significant association was the proportion of ADC-rCBV ROI in the nonenhancing area *(NE)* (area under the receiver operating characteristic curve *[AUC]*, 0.717; *P* = .034). *CE* = contrast-enhancing area.

reported here, where an elevated Cho/NAA ratio or index was identified outside the area of contrast enhancement (16), and has even led to identification of tumor extent outside the area of contrast enhancement (41). With regard to the nonenhancing region, Jain et al (27) previously reported elevated rCBV in the nonenhancing region to be associated with poor survival. However, they identified nonenhancement as a 1-cm fluid-attenuated inversion recovery border around the region of contrast enhancement; whereas in our study, we identified the nonenhancing region as the entire area of fluid-attenuated inversion recovery hyperintensity surrounding the contrast-enhancing region. Previous work that used low ADC, high rCBV, and Cho and NAA for survival analyses did not analyze regional low ADC that intersected with high rCBV, and all parameters were considered individual variables (16).

Our study had limitations. The imaging thresholds reported in this article are derived from our own population and were not independently tested. Since they are from one center and are from retrospective data analysis, additional studies will be needed for confirmation. The $^1$H MR spectroscopy voxels were large in comparison with the ADC and rCBV voxels. Histologic data for this cohort were not obtained, as the brain shift during surgery did not allow for accurate image-guided data acquisition. Finally, our study protocol did not include quantitative T1 or T2 parameters.

In summary, as the nonenhancing component is typically left behind after surgery, studies of this nature may be useful in identifying subregions that would be better suited for targeted boost radiation therapy volumes or potential sites of extended surgical resection of GBM.

**References**

1. Sottoriva A, Spiteri I, Piccirillo SG, et al. Intratumor heterogeneity in human glioblastoma reflects cancer evolutionary dynamics. Proc Natl Acad Sci U S A 2013;110(10):4009–4014.

2. Kelly PJ, Daumas-Duport C, Kispert DB, Kall BA, Scheithauer BW, Illig JJ. Imaging-based stereotaxic serial biopsies in untreated intracranial glial neoplasms. J Neurosurg 1987;66(6):865–874.

3. Oppitz U, Maessen D, Zunterer H, Richter S, Flentje M. 3D-recurrence-patterns of glioblastomas after CT-planned postoperative irradiation. Radiother Oncol 1999;53(1):53–57.

4. Chan JL, Lee SW, Fraass BA, et al. Survival and failure patterns of high-grade gliomas after three-dimensional conformal radiotherapy. J Clin Oncol 2002;20(6):1635–1642.

5. Sugahara T, Korogi Y, Kochi M, et al. Correlation of MR imaging-determined cerebral blood volume maps with histologic and angiographic determination of vascularity of gliomas. AJR Am J Roentgenol 1998;171(6):1479–1486.

6. Sugahara T, Korogi Y, Kochi M, Ushio Y, Takahashi M. Perfusion-sensitive MR imaging of gliomas: comparison between gradient-echo and spin-echo echo-planar imaging techniques. AJNR Am J Neuroradiol 2001;22(7):1306–1315.

7. Hilario A, Ramos A, Perez-Nuñez A, et al. The added value of apparent diffusion coefficient to cerebral blood volume in the preoperative grading of diffuse gliomas. AJNR Am J Neuroradiol 2012;33(4):701–707.

8. Caseiras GB, Chheang S, Babb J, et al. Relative cerebral blood volume measurements of low-grade gliomas predict patient outcome in a multi-institution setting. Eur J Radiol 2010;73(2):215–220.

9. Barajas RF Jr, Phillips JJ, Parvataneni R, et al. Regional variation in histopathologic features of tumor specimens from treatment-naive glioblastoma correlates with anatomic and physiologic MR Imaging. Neuro-oncol 2012;14(7):942–954.

10. Gupta RK, Cloughesy TF, Sinha U, et al. Relationships between choline magnetic resonance spectroscopy, apparent diffusion coefficient and quantitative histopathology in human glioma. J Neurooncol 2000;50(3):215–226.

11. Khayal IS, Crawford FW, Saraswathy S, et al. Relationship between choline and apparent diffusion coefficient in patients with gliomas. J Magn Reson Imaging 2008;27(4):718–725.

12. Sijens PE, Heesters MA, Enting RH, et al. Diffusion tensor imaging and chemical shift imaging assessment of heterogeneity in low grade glioma under temozolomide chemotherapy. Cancer Invest 2007;25(8):706–710.

13. Sugahara T, Korogi Y, Kochi M, et al. Usefulness of diffusion-weighted MRI with echo-planar technique in the evaluation of cellularity in gliomas. J Magn Reson Imaging 1999;9(1):53–60.

14. Crawford FW, Khayal IS, McGue C, et al. Relationship of pre-surgery metabolic and physiological MR imaging parameters to survival for patients with untreated GBM. J Neurooncol 2009;91(3):337–351.

15. Oh J, Henry RG, Pirzkall A, et al. Survival analysis in patients with glioblastoma multiforme: predictive value of choline-to-N-acetylaspartate index, apparent diffusion coefficient, and relative cerebral blood volume. J Magn Reson Imaging 2004;19(5):546–554.

16. Saraswathy S, Crawford FW, Lamborn KR, et al. Evaluation of MR markers that predict survival in patients with newly diagnosed GBM prior to adjuvant therapy. J Neurooncol 2009;91(1):69–81.

17. Law M, Yang S, Wang H, et al. Glioma grading: sensitivity, specificity, and predictive values of perfusion MR imaging and proton MR spectroscopic imaging compared with conventional MR imaging. AJNR Am J Neuroradiol 2003;24(10):1989–1998.

18. Price SJ, Peña A, Burnet NG, et al. Tissue signature characterisation of diffusion tensor abnormalities in cerebral gliomas. Eur Radiol 2004;14(10):1909–1917.

19. Price SJ, Jena R, Burnet NG, Carpenter TA, Pickard JD, Gillard JH. Predicting patterns of glioma recurrence using diffusion tensor imaging. Eur Radiol 2007;17(7):1675–1684.

20. Ellingson BM, Malkin MG, Rand SD, et al. Validation of functional diffusion maps (fDMs) as a biomarker for human glioma cellularity. J Magn Reson Imaging 2010;31(3):538–548.

21. Price SJ, Green HA, Dean AF, Joseph J, Hutchinson PJ, Gillard JH. Correlation of MR relative cerebral blood volume measurements with cellular density and proliferation in high-grade gliomas: an image-guided biopsy study. AJNR Am J Neuroradiol 2011;32(3):501–506.

22. McKnight TR, Lamborn KR, Love TD, et al. Correlation of magnetic resonance spectroscopic and growth characteristics within Grades II and III gliomas. J Neurosurg 2007;106(4):660–666.

23. Guo J, Yao C, Chen H, et al. The relationship between Cho/NAA and glioma metabolism: implementation for margin delineation of cerebral gliomas. Acta Neurochir (Wien) 2012;154(8):1361–1370; discussion 1370.

24. Croteau D, Scarpace L, Hearshen D, et al. Correlation between magnetic resonance spectroscopy imaging and image-guided biopsies: semiquantitative and qualitative histopathological analyses of patients with untreated glioma. Neurosurgery 2001;49(4):823–829.

25. McKnight TR, von dem Bussche MH, Vigneron DB, et al. Histopathological validation of a three-dimensional magnetic resonance spectroscopy index as a predictor of tumor presence. J Neurosurg 2002;97(4):794–802.

26. Piccirillo SG, Dietz S, Madhu B, et al. Fluorescence-guided surgical sampling of glioblastoma identifies phenotypically distinct tumour-initiating cell populations in the tumour mass and margin. Br J Cancer 2012;107(3):462–468.

27. Jain R, Poisson LM, Gutman D, et al. Outcome prediction in patients with glioblastoma by using imaging, clinical, and genomic biomarkers: focus on the nonenhancing component of the tumor. Radiology 2014;272(2):484–493.

28. Ellingson BM, Lai A, Nguyen HN, Nghiemphu PL, Pope WB, Cloughesy TF. Quantification of nonenhancing tumor burden in gliomas using effective T2 maps derived from dual-echo turbo spin-echo MRI. Clin Cancer Res 2015;21(19):4373–4383.

29. Leu K, Enzmann DR, Woodworth DC, et al. Hypervascular tumor volume estimated by comparison to a large-scale cerebral blood volume radiographic atlas predicts survival in recurrent glioblastoma treated with bevacizumab. Cancer Imaging 2014;14:31.

30. Sanai N, Polley MY, McDermott MW, Parsa AT, Berger MS. An extent of resection threshold for newly diagnosed glioblastomas. J Neurosurg 2011;115(1):3–8.

31. Iliadis G, Kotoula V, Chatzisotiriou A, et al. Volumetric and MGMT parameters in glioblastoma patients: survival analysis. BMC Cancer 2012;12:3.

32. Hegi ME, Diserens AC, Gorlia T, et al. MGMT gene silencing and benefit from temozolomide in glioblastoma. N Engl J Med 2005;352(10):997–1003.

33. Cohen AL, Holmen SL, Colman H. IDH1 and IDH2 mutations in gliomas. Curr Neurol Neurosci Rep 2013;13(5):345.

34. Vogelbaum MA, Jost S, Aghi MK, et al. Application of novel response/progression measures for surgically delivered therapies for gliomas: Response Assessment in Neuro-Oncology (RANO) Working Group. Neurosurgery 2012;70(1):234–243; discussion 243–244.

35. Price SJ, Young AM, Scotton WJ, et al. Multimodal MRI can identify perfusion and metabolic changes in the invasive margin of glioblastomas. J Magn Reson Imaging 2016;43(2):487–494.

36. Kreis R. Issues of spectral quality in clinical 1H-magnetic resonance spectroscopy and a gallery of artifacts. NMR Biomed 2004;17(6):361–381.

37. Boxerman JL, Schmainda KM, Weisskoff RM. Relative cerebral blood volume maps corrected for contrast agent extravasation significantly correlate with glioma tumor grade, whereas uncorrected maps do not. AJNR Am J Neuroradiol 2006;27(4):859–867.

38. Catalaa I, Henry R, Dillon WP, et al. Perfusion, diffusion and spectroscopy values in newly diagnosed cerebral gliomas. NMR Biomed 2006;19(4):463–475.

39. Ryu YJ, Choi SH, Park SJ, Yun TJ, Kim JH, Sohn CH. Glioma: application of whole-tumor texture analysis of diffusion-weighted imaging for the evaluation of tumor heterogeneity. PLoS One 2014;9(9):e108335.

40. Barajas RF Jr, Hodgson JG, Chang JS, et al. Glioblastoma multiforme regional genetic and cellular expression patterns: influence on anatomic and physiologic MR imaging. Radiology 2010;254(2):564–576.

41. Pirzkall A, McGue C, Saraswathy S, et al. Tumor regrowth between surgery and initiation of adjuvant therapy in patients with newly diagnosed glioblastoma. Neuro-oncol 2009;11(6):842–852.